2003-01-2988

Prediction of Aircraft Safety Performance in Complex Flight Situations

Ivan Y. Burdun
[obsolete affiliation information removed]

ABSTRACT

A generic situational model of the “pilot (automaton) – aircraft – operational environment” system is employed as a 'virtual safety test article'. The goal is to identify *a priori* potentially catastrophic, safe and interim developments in the system behavior in complex (multi-factor) flight situations. Distinguishing features of the technique include: affordability and autonomy of experimentation (a pilot and special hardware are not required), easy planning and fast-time simulation of a large number of non-standard flight scenarios on a computer, and automated assessment and classification of 'flights' using formalized safety criteria. A software tool called VATES, which implements this technique, is demonstrated. Several new graphic-analytical formats designed for system safety knowledge mapping are introduced using realistic situation examples.

INTRODUCTION

PROBLEM

Flight safety is essentially a systemic property. It is determined by the three constituents of the “pilot (automaton) - aircraft - operational environment” system (the system), namely [1, 2]: the human pilot or/and automaton, the flying vehicle with its subsystems, and weather and other external conditions. Given a certain rare combination of several demanding operating factors and, possibly, hidden design flaws, a chain of strong cause-and-effect links may spontaneously develop in the system behavior. This often leads the vehicle irreversibly towards a catastrophe/incident. 'Chain reaction' flight situations exhibit the following *common features* [2]:

- a 'snow-ball' of critical events and processes (accumulation of the 'critical mass' of complexity)
- cross-coupling effects of several operating and design factors
- cause-and-effect inertia
- pilot-automation incoherence, and
- existence of a recovery point – the last opportunity to restore a safe flight regime.

As a result, the aircraft may inadvertently enter an anomalous sub-domain of flight modes with a small, unsteady safety margin and insufficient chances of recovery [2]. Under such circumstances, the system state transitions are very sensitive to the type and strength of the contributing factors. If this branching property is ignored in the aircraft design, test and evaluation (T&E), a 'chain reaction' type accident pattern may be literally pre-programmed in the system behavior [1-4]. Note that after a recovery point, *any* control input is likely to be inadequate or 'erroneous'. Obviously, non-standard flight scenarios prone to 'chain reactions' must be identified and examined before operation. Therefore, the *problem under study* can be formulated as follows. How to test and evaluate the system's safety performance in complex (multi-factor) flight situations in advance, i.e. not based on flight accident statistics?

PRESENT PRACTICE

At present, however, many non-standard flight situation patterns with substantial deviations from the norm remain unexplored due to time and budget constraints [5]. In addition, existing T&E and safety analysis techniques exhibit limitations when modeling *multi-factor* flight cases. As a result, ‘chain reaction’ accidents do happen in operation though their theoretical probability of occurrence is negligible. It is also difficult to reconstruct a ‘chain reaction’ accident situation and analyze its ‘what-if neighborhood’. The causes of several catastrophes with strong system dynamics features remain unclear for a long time, or the results of their investigation are still controversial. These facts enable a formulation of, perhaps, the *most general explanation of aviation catastrophes* - as a non-eliminated discrepancy between previously unknown non-standard (dangerous) and recommended (safe) scenarios of flight.

~~Note~~. In some flight safety analyses, there is a tendency of attributing a ‘chain reaction’ accident mainly to a so called 'pilot error' or/and to some difficult-to-measure demanding weather condition. However, this approach cannot be accepted as irreproachable, both scientifically and legally. In a multi-factor, chaining situation, the system behavior may exhibit features of both normal and

chaotic dynamics. It is a characteristic property of such complex systems that, given a boundary state, a small change of input yields a large transition of the system state. In addition, if flight proceeds at a 'corner' of the aircraft's performance envelope, the system may suddenly reveal hidden weaknesses of its all three components. Such 'corners', if coupled with other complications of flight, are difficult to identify and test prior to an accident [3]. "Over-automation" makes aircraft even more sensitive to the effect of multiple operating conditions and thus prone to 'chain reactions' [2]. This happens, in particular, because modern automatic and manual aircraft control scenarios cannot address all combined effects of various non-standard circumstances of flight. Therefore, a deep analysis of the system dynamics and logics in a complex flight situation would be useful to help prevent catastrophic patterns from occurring in future operations.

SOLUTION APPROACH

A *knowledge-centered approach* to studying safety performance of complex (multi-factor) flight domains is being developed. In the study, a mathematical model substitutes the real system. This is a generic autonomous situational model of the 'pilot (automaton) - aircraft - operational environment' system behavior [1, 4]. The adjectives 'autonomous' and 'situational' mean that a human pilot's decision-making processes and non-standard flight scenarios are described mathematically along with the vehicle non-linear flight mechanics. The adjective 'generic' means that the model's equations and algorithms can be tuned in to a specific vehicle/project using its 'parametric definition' database as input. As a result, flexible planning and fast-time simulation of various realistic 'what-if' cases on computer can be carried out directly by a designer, certification engineer, safety expert, or a pilot.

The overall goal in the solution approach is to fill the gap in the specialist's 'internal knowledge base' on the system's safety performance under multiple operating conditions. A broad set of non-standard scenarios of flight can be examined on a PC in compliance with pertinent airworthiness requirements or other inputs. This is expected to help identify, learn and remedy potentially unsafe anomalies in the system behavior in advance.

'VIRTUAL' FLIGHT TEST AND EVALUATION

DEFINITION

A technique of experimentation with the system model on computer is called *'virtual' flight test and evaluation* (VFT&E) [3, 5]. In it, several methods are used in concert: aircraft applied aerodynamics, flight mechanics, numeric simulation, fuzzy sets, situational control, artificial intelligence, computer graphics, and some other. The technique helps automate and accelerate substantially the process of examining complex flight domains, increase the volume of up-front information about the system safety performance in 10^2-10^3 times, and simultaneously reduce the cost of obtaining such information.

TOOL

The VFT&E technique has been implemented in a proprietary software tool called VATES. The abbreviation stands for the Virtual Autonomous Test and Evaluation Simulator, which is employed here as a 'virtual flight safety test-bed' [4]. The following main components constitute VATES: a discrete-continuous scenario-based model of a human pilot's decision-making tactics, a generalized flight situation model, a generalized non-linear model of the six-degree-of-freedom motion of a fixed-wing aircraft, and a number of heterogeneous models of key operating and design factors. The latter set describes the following effects: a human pilot's control errors/variations or inattention; onboard hardware failures (engine(s), controls, etc.) and software errors (in automatic control systems); demanding weather conditions - wind of any 3-D profile (wind-shear, 'microburst', cross-wind, etc.), atmospheric turbulence, heavy rain/shower, aircraft surface icing, runway's surface condition (water/snow-covered, wet, dry, etc.), runway slope, elevation and dynamics, non-standard atmospheric conditions (temperature, pressure); variations in the airplane's configuration, mass, and center-of-gravity location; and a 'parametric definition' of the vehicle/project under study. The tool also includes a set of new concepts and algorithms that automate the process of planning, mapping, classification and assessment of flight scenarios using formalized safety criteria. As a result, the user can perform fast-time 'virtual safety test' experiments on a plain PC based on a 'what …, if …?' principle. The objective is to examine a complex, multi-factor flight domain, both in-depth and in-breadth, and thus obtain a more detailed 'portrait' of the system's safety performance in advance.

PROCESS

Fig. 1 depicts a general layout of the VFT&E process. It consists of the following *research steps*: 'tune in' the generalized system model to a given project/vehicle; design a plan of 'what-if' simulation experiments including a flight situation scenario, an operational hypothesis, and a set of output knowledge-mapping formats; run autonomous simulation experiments using a 'micro-structural' model of flight; run a series of simulation experiments using a 'macro-structural' model of flight; analyze the model's output results; develop feedback recommendations on the system safety to designers and/or pilots.

The main objects of the VFT&E process include: a database (**5**) of the aircraft model aerodynamics and

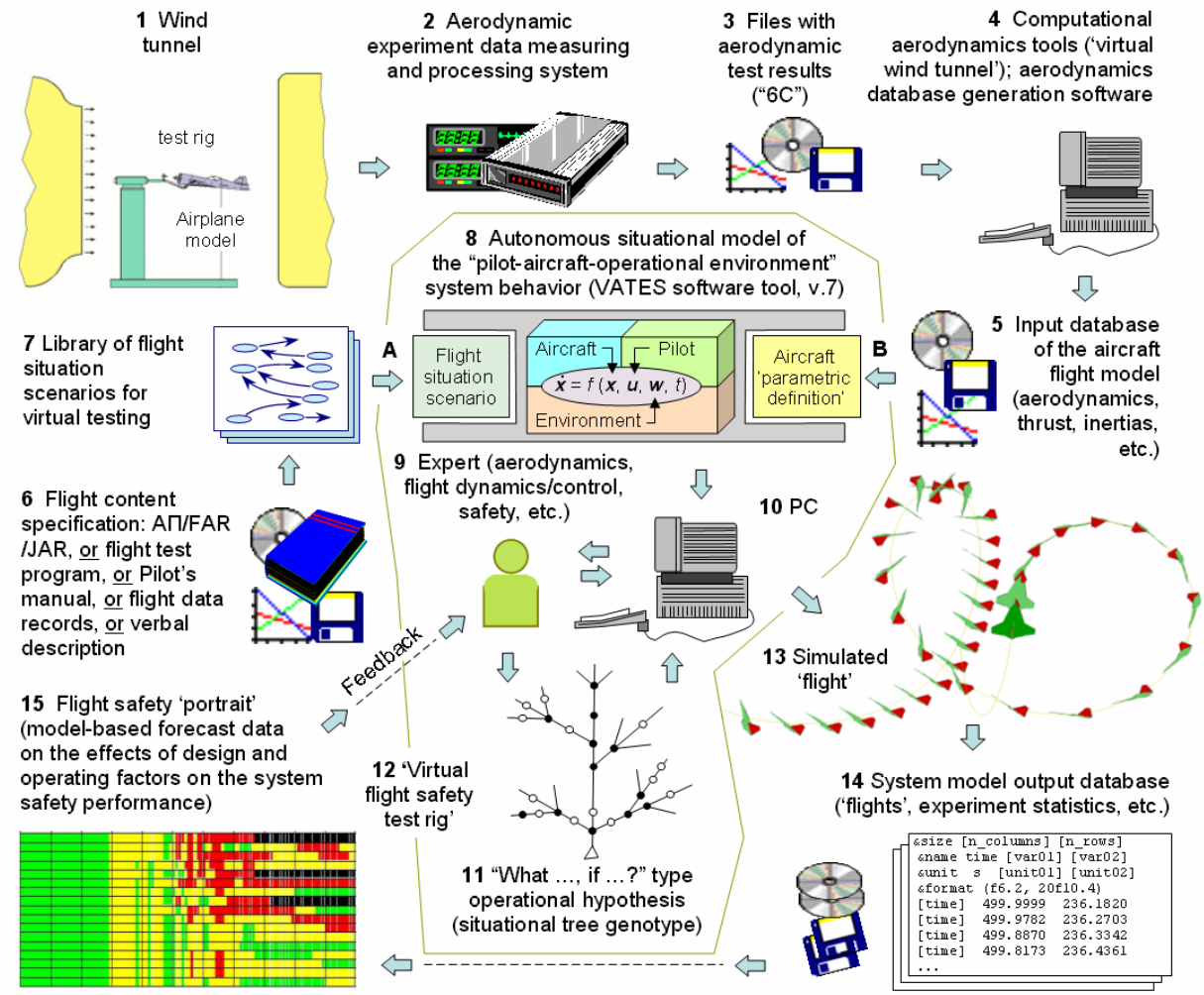

Fig. 1: General layout of the 'virtual flight safety test and evaluation' process

other input characteristics (thrust, mass, geometry, inertias, etc. - it is called a *'parametric definition'* of the vehicle [5]) together with the database build-up and verification techniques (**1**-**4**); a generalized situational model (**8**) of the system behavior, which consists of the three main groups of algorithms (flight mechanics and control, human piloting, and operational environment); a library (**7**) of flight scenarios for testing in autonomous simulation; a researcher (**9**) - an aerodynamicist, designer, certification engineer, safety expert, or a pilot - who develops a 'what …, if …?' operational hypothesis (**11**) and examines it in simulation experiments (**10**).

DATA

The developed autonomous situational model of flight requires two input data flows, **A** and **B** (ref. Fig. 1). Flow **A** contains files with a flight scenario selected for virtual testing. In order to construct that scenario, *one* of the following sources (**6**) of flight content specification is required: pertinent airworthiness requirements - FAR, JAR, АП, etc., or a test program, or a Pilot's Manual, or actual flight test/operation records, or a verbal description of a flight situation. Flow **B** represents another set of input files containing a 'parametric definition' of the vehicle under testing. It is formed using wind-tunnel experiment data (**3**) and results of calculation of the vehicle's aerodynamic and other source characteristics (**4**). The model's output unit is one *'flight'* (**13**) – a set of tables and other electronic files that contain results of one simulation run. A collection of 'flights' constitutes the model's output database (**14**). Finally, a detailed 'portrait' of the system's safety performance (**15**) is formed based on these simulation results. The above-listed data sets are generated and processed automatically. The model can be tuned in to a specific vehicle type and safety research task within one-two weeks (i.e. when input flows **A** and **B** are ready) provided that data sources **4** and **6** are available.

'MICRO-STRUCTURE' OF FLIGHT

According to the developed methodology [2], flight is formalized and simulated in the system model at two

interrelated levels (**Fig. 2**). These are the 'micro-structure' of flight (a single-situation model) and the 'macro-structure' of flight (a situation-set model).

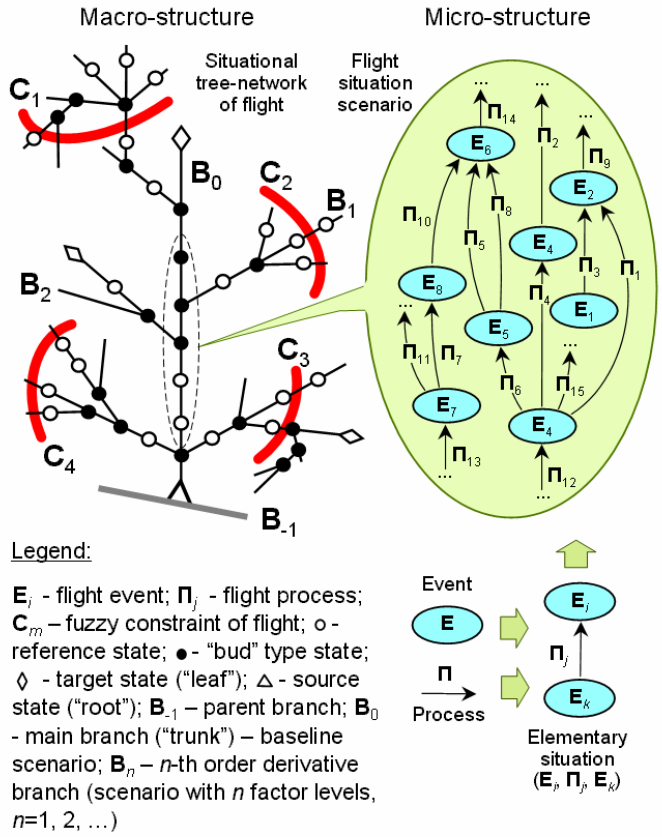

Fig. 2: Relationship between micro- and macro-structure of flight implemented in the generic system model

The *'micro-structure' of flight* is represented by a flight scenario. The *flight [situation] scenario*, **S**, is a plan of a flight situation of interest. It is described and depicted as a directed graph [1, 4, 5]. The latter is defined by the following two sets: $\Omega(\mathbf{E})$ – a *calendar of flight events* **E** (the graph's vertices, or discrete components of **S**) and $\Omega(\mathbf{\Pi})$ – a *united list of flight processes* **Π** (the graph's arcs, or continuous components of **S**). Thus, $\mathbf{S} = \Omega(\mathbf{E}) \cup \Omega(\mathbf{\Pi})$, where:

$$\Omega(\mathbf{\Pi}) = \Omega(\mathbf{D}) \cup \Omega(\mathbf{B}) \cup \Omega(\mathbf{F}) \cup \Omega(\mathbf{T}) \cup \Omega(\mathbf{P}) \cup \Omega(\mathbf{O}) \cup \Omega(\mathbf{W}) \cup \Omega(\mathbf{L}) \cup \Omega(\mathbf{R}) \cup \Omega(\mathbf{I}) \cup \Omega(\mathbf{Y}) \cup \ldots. \quad (1)$$

In union (1), $\Omega(\square)$ is a list of $\square$-type processes. The process types are as follows: the *vehicle's dynamics* (**D**), *on-board system function* (**B**) and *failure* (**F**), *piloting task* (**T**), *control procedure* (**P**), *system state observer* (**O**), *wind* (**W**), *turbulence* (**L**), *rain* (**R**), *icing* (**I**), *runway's surface condition* (**Y**), etc. [1].

Triples ($\mathbf{E}_i$, $\mathbf{\Pi}_j$, $\mathbf{E}_k$) constitute *elementary situations*. These are 'building blocks', which are combined together in **S** to describe the content of a situation of almost any type and complexity - catastrophic, test, non-standard, training, normal, etc. Note that the electronic files, which represent sets $\Omega(\mathbf{E})$ and $\Omega(\mathbf{\Pi})$, constitute the model's input data flow (**A**) – ref. Fig. 1. In the model, examined operating and design factors are introduced as variations in the attributes and structure of flight scenario **S**. This is a simple, yet efficient technique that enables the user to quickly plan various (complex and standard) flight scenarios. It has been tested on 22 aircraft types/projects and 500+ flight scenario types for all main phases of flight and key operating conditions. Thus, the developed formalism of discrete-continuous scenarios helps simulate heterogeneous events and processes of flight in a coherent, integrated fashion.

'MACRO-STRUCTURE' OF FLIGHT

In real operations, however, flights may differ from recommended, ideal scenarios. It is also hard to find two identical flights. A set of variants of some source scenario that are generated according to a certain rule forms the *'macro-structure' of flight* (ref. Fig. 2). This concept is expedient to model, depict and analyze as a *situational tree*, ***T***. The tree's *trunk* $\boldsymbol{B}_0$ stands for a 'flight', which corresponds to a baseline (ideal, or not) scenario **S**. A higher-level *derivative branches* $\boldsymbol{B}_i$ are formed by introducing new operating and/or design factors into a lower-level scenario, i=1, 2, … Therefore, the development logic of each flight path-branch $\boldsymbol{B}_i$ in ***T*** is entirely determined by its internal scenario and the system dynamics.

One of the problems with multi-attribute dynamic data structures, such as trees, is the 'curse of dimensionality'. The tool enables the user to 'plant' comprehensive yet economical (memory-wise) flight situation trees in autonomous simulation experiments using the 'micro-model' as a branch generator. This can be achieved through the process of 'fuzzification' of the system numeric states using fuzzy sets. In addition, the following notions from botany and biology are employed (see Fig. 2): 'root', 'bud', 'leaf', 'crown', and 'genotype' [2]. The *tree's genotype*, or *operational hypothesis*, **Γ**, is a special rule of combining operating and design factors in the tree's structure. In other words, **Γ** is a tree growth control technique, which implements the tree's crown shaping, directing, trimming and other functions. In a situational tree, time t runs along each branch, from the tree's *root* (△) towards *leaves* (◊). New branches are implanted in *'bud'*-type states (●). Reference states (○) are periodically inserted into ***T*** to be able to monitor and record the system's interim dynamics. The thick arcs shown across branches denote violated constraints ***C*** - ref. Fig. 2.

It can be shown [2, 3] that the above-described principles of construction of formal scenarios and situational trees of flight are compatible with a human pilot's 'internal model' of a complex flight situation domain. Obviously, there exist optimal, sub-optimal,

acceptable and unacceptable (unsafe) 'genotypes' of a specialist's knowledge model of flight. A carefully programmed artificial knowledge tree structure is therefore needed to properly thread (exemplify) a sub-domain of multi-factor flight situations at constraints. The objective is to help the specialist to reveal the system's safety topology under non-standard conditions with a minimal consumption of resources.

KNOWLEDGE MAPPING FORMATS

A set of graphic-analytical formats designed to map the system safety related knowledge of a human pilot (or other flight professional) can be generated automatically using VATES. The following *safety knowledge-mapping formats* are introduced and demonstrated in this paper: 'flight situation scenario', 'fuzzy flight constraint', 'partial flight safety spectrum', 'integral flight safety spectrum', 'situation complexity build-up diagram', 'time-history of flight events', 'fuzzy flight constraint violation/restoration chronology and interdependence chart', 'situational tree', 'situational tree's complexity build-up diagrams', 'flight safety performance cause-and-effect map', 'family of situational tree's flight safety spectra', 'distribution of a tree's flights due to safety performance (equal-safety cluster table and safety sector diagram)', and 'safety [performance] window'. The tool also incorporates algorithms to calculate 'flight safety indices' and partition a tree/set of simulated 'flights' (scenarios) onto equal-safety situation clusters using five 'safety categories' [3]. Another subset of flight safety knowledge mapping formats has been demonstrated in [2, 4] including: 'flight scenario time-history', '3-D flight path - roll ribbon', '3-D flight path - roll ribbon - flight events diagram', '4-D flight movie', 'situation forecast display', and 'flight safety indicator'.

The following two sections contain a more detailed introduction to the developed framework of the system model-based flight safety analysis on the micro- and macro-levels. In this presentation, an advanced turboprop commuter airplane project is being employed as an example [3].

'MICRO-STRUCTURAL' ANALYSIS EXAMPLE

SITUATION SCENARIO

Fig. 3 depicts a realistic flight scenario graph **S**. It describes the following non-standard flight situation: 'Normal takeoff and initial climb under 'very strong' wind-shear and variations/errors while maintaining commanded flight-path and bank angles, θ_G and γ_G, in climb'. The directed graph **S** is defined by the following two sets: $\Omega(\mathbf{E})=\{\mathbf{E}_1, \ldots, \mathbf{E}_{12}\}$ and $\Omega(\mathbf{\Pi})=\{\mathbf{T}_1, \ldots, \mathbf{T}_4, \mathbf{P}_1, \ldots, \mathbf{P}_4, \mathbf{W}_1\}$, where $\mathbf{E}_i$ is a flight event, $\mathbf{T}_j$ is a 'piloting task' (a multi-step piloting process that requires continuous observations of the system state), $\mathbf{P}_k$ is a 'control procedure' (an 'on-off' type single control action without continuous observation), and $\mathbf{W}_1$ is a 2-D 'very strong' wind-shear profile derived from an accident [1]; $i \in \{1, \ldots, 12\}$, $j,k \in \{1, \ldots, 4\}$.

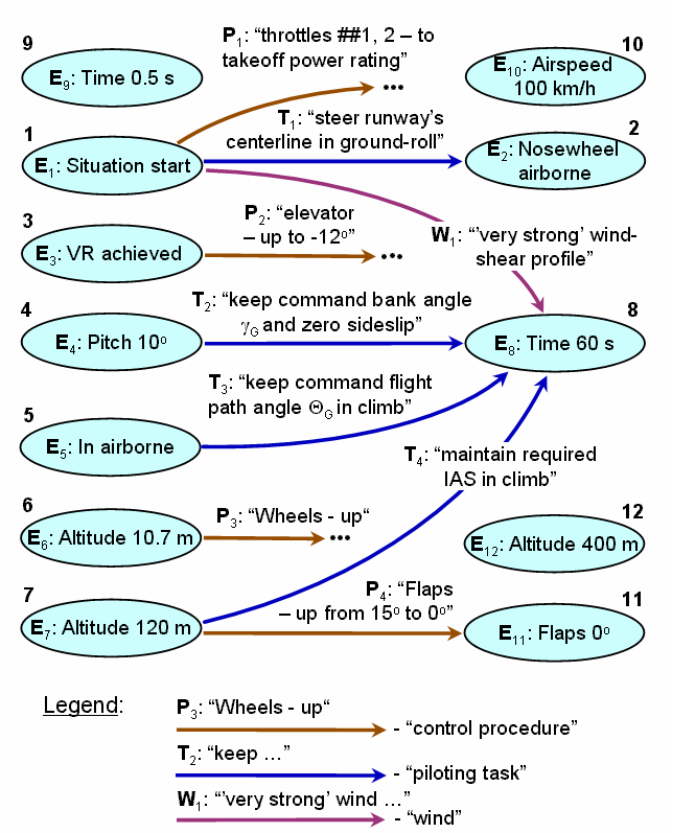

Fig. 3: Flight scenario **S**: "Normal takeoff, initial climb, 'very strong' wind-shear, flight path Θ_G and bank γ_G variations/errors"

FLIGHT AND CONTROL LOGIC

The scenario graph shown in Fig. 3 is interpreted as follows. The examined flight situation starts at event-node $\mathbf{E}_1$. The 'silicon pilot' shifts the aircraft engines' control levers to a takeoff power rating setting; this is done by means of control procedure-arc $\mathbf{P}_1$. Simultaneously, at $\mathbf{E}_1$, the pilot model begins to steer the runway's centerline in ground-roll (piloting task $\mathbf{T}_1$). This process is finished at event $\mathbf{E}_2$: 'nose wheel airborne'. At rotation speed V_R (event $\mathbf{E}_3$) elevator goes up to rotate the airplane by means of $\mathbf{P}_2$. When the airplane's attitude in pitch reaches about $+10^o$ ($\mathbf{E}_4$) another piloting task, $\mathbf{T}_2$, is launched to maintain the commanded (not necessarily optimal) bank angle γ_G and zero sideslip (β=0). When the airplane is in airborne (signaled by $\mathbf{E}_5$) the pilot model modifies its control tactics and establishes a certain (not necessarily optimal) flight-path angle Θ_G ($\mathbf{T}_3$). Beginning from event $\mathbf{E}_6$, wheels are commanded to retract ($\mathbf{P}_3$). At an altitude of about 120 meters ($\mathbf{E}_7$) flaps are retracted ($\mathbf{P}_4$) to zero (indicated by $\mathbf{E}_{11}$), and a new piloting task ($\mathbf{T}_4$) starts to keep the airspeed constant during climb. In addition, a 'very strong' wind-shear profile (process $\mathbf{W}_1$) affects the entire 'flight' - from $\mathbf{E}_1$ to

$\mathbf{E}_8$. The examined situation ends at event $\mathbf{E}_8$. Note also that the remaining three events {$\mathbf{E}_9$, $\mathbf{E}_{10}$, $\mathbf{E}_{12}$} from $\Omega(\mathbf{E})$ have no processes associated with them in **S**. Such (stand-alone) events are used to mark some characteristic states in the system behavior. They are also useful for simulation data recording and statistics gathering (i.e. as 'reference' ○ and 'leaf' ◊ states), or for scenario concatenation and branching in ***T*** (as 'bud' ● and 'root' △ states).

Therefore, the notion of flight scenario helps formalize heterogeneous cause-and-effect relationships in the system model by means of generic objects of two types: 'event' and 'process'. It is essential that parametric variations in the events and processes constituting **S**, such as θ_G, γ_G, etc., do not affect its overall structure.

FUZZY CONSTRAINTS

In order to make conclusions on the system's safety performance, it is necessary to define its operational limits. In the model, the concept of fuzzy constraint first introduced by Lotfi A. Zadeh [7] is employed (**Fig. 4**). Flight constraints are formalized using a binary membership criterion ('yes', or 'no'), such as, for example, constraint ***C***: 'α<12.5°' - ref. Fig. 4(b). Then, according to this, precisely defined constraint ***C***, one boundary value of the angle of attack (say, α=12.49°) is treated as acceptable (safe), whilst another - a slightly higher - boundary value (for instance, α=12.51°) is already not. Obviously, this is not a practically correct statement. On the contrary, *fuzzy constraint* ***C*** describes transitions from unacceptable (unsafe) values of a monitored system's state variable x to acceptable (safe) ones *gradually*, not as a sharp change of membership - see Fig. 4(c). In other words, there exists a region of partial membership of variable x values to fuzzy set-constraint ***C*** - $\mu_C(x)\in]0;\ 1[$. For the commuter airplane example fuzzy constraints placed upon selected key state variables x_k at takeoff are specified in [4], where $x_k \in \{V_{IAS}, \beta, n_z, \dot{E}, E, N, \gamma, \vartheta, V_{zg}, \alpha, k_{LG}, \delta_e, \delta_a, \delta_r, \delta_F\}$. Therefore, the notion of fuzzy set helps formalize inherently imprecise (essentially of non-statistical nature) constraints in mathematically accurate and ergonomically compatible terms.

SAFETY PALETTE

The four characteristic zones of the definition range of variable x under its fuzzy constraint membership function plot are color-coded using the following *safety colors* or levels [1]: ξ_G – *green* ('norm'), ξ_A – *amber* ('attention'), ξ_R – *red* ('danger'), and ξ_B – *black* ('fatal'). There may be other, interim or special, safety/performance colors too (e.g., to denote goal states). If the algorithm of its fuzzy constraint violation check up is temporarily 'switched off' for some variable x, then a *gray/white* color-code ξ_W is assigned to x. It means that the system's partial safety status along x is 'unknown' at given time instants. Therefore, the overall *safety palette*, {ξ_G, ξ_A, ξ_R, ξ_B, ξ_W, …}, can be designed to reflect pertinent airworthiness requirements, specific flight conditions, aircraft design and operation limits, and professional opinions of flight experts regarding acceptable, marginal and critical states of the system. These notions will be used below to construct safety spectra and calculate safety indices of simulated 'flights'.

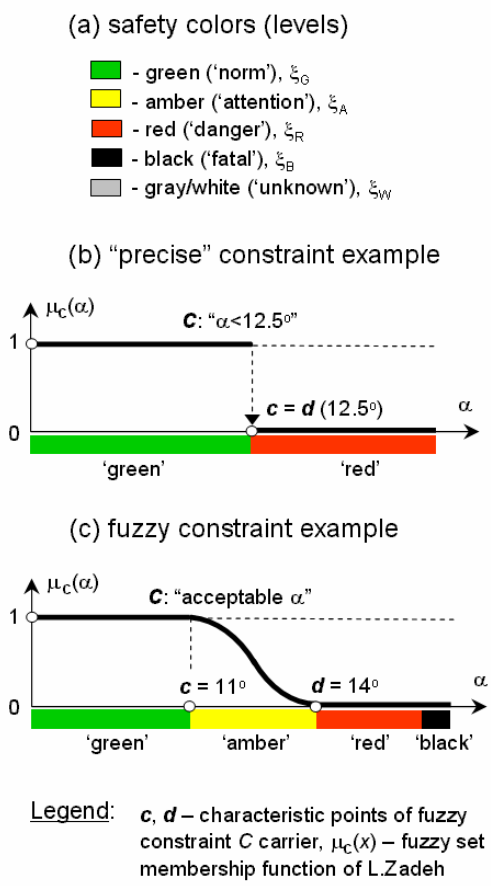

Fig. 4: Safety colors (levels), "precise" vs. fuzzy constraints of flight

PARTIAL SAFETY SPECTRUM

The *partial flight safety spectrum* [1], Σ_k, is a graphic time-history, or a color-coded bar, that shows how the safety status of some monitored variable x_k changes during a flight situation. In order to construct partial safety spectra Σ_k, k=1, …, p, it is required to check the degree of violation of corresponding fuzzy constraints $\mathbf{C}(x_k)$. Then, for each x_k, its current value $x_k(t)$ is to be associated with color code $\xi(x_k(t))$, $\xi(x_k(t))\in\{\xi_G, \xi_A, \xi_R, \xi_B, \xi_W, \ldots\}$ – ref. Fig. 4(a) and 4(c). Note that $t\in[t(\mathbf{E}_*);t(\mathbf{E}^*)]$ in $\xi(x_k(t))$, where $\mathbf{E}_*$ is the *start event*, and $\mathbf{E}^*$ is the *stop event* of a flight situation under examination. In scenario **S** we have: $\mathbf{E}_*\equiv\mathbf{E}_1$ and $\mathbf{E}^*\equiv\mathbf{E}_8$. The set {$\xi_G$, ξ_A, ξ_R, ξ_B, ξ_W, …} must be an agreed safety palette for all monitored variables x_k and all segments of a flight situation under study, k=1, …, p. **Fig. 5** shows

examples of the partial safety spectra, Σ_1, … Σ_{20}, constructed for flight situation $\boldsymbol{F}_{2782}$: "Normal takeoff and initial climb under 'very strong' wind-shear, Θ_G=+16° and γ_G=+22.5°". Note that 'flight' $\boldsymbol{F}_{2782}$ has been generated according to generic scenario **S** given Θ_G=16° and γ_G=22.5°. Gray coloring of some parts of spectrum Σ_k means that the system's safety performance is not monitored there, k=1, …, 20.

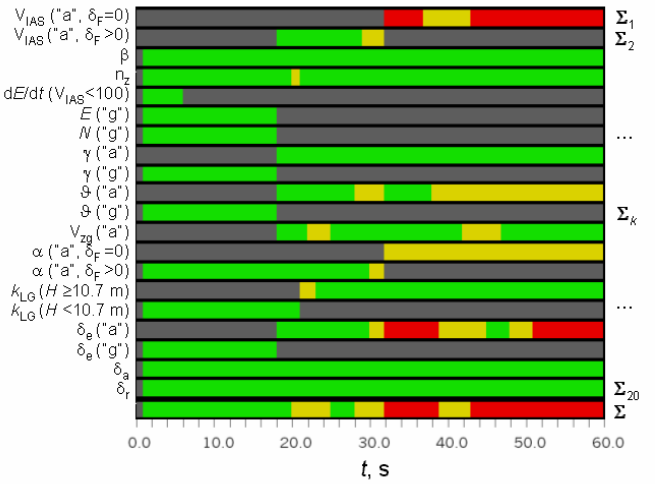

Legend:

Safety colors – ref. Fig. 4; Σ_k – partial safety spectrum constructed for variable x_k, k = 1, …, p; p = 20; Σ - integral safety spectrum of 'flight'; "a" – airborne phase, "g" – ground-roll phase

Fig. 5: Partial and integral safety spectra - 'flight' $\boldsymbol{F}_{2782}$: "Normal takeoff, initial climb at Θ_G=16° and γ_G=+22.5° under 'very strong' wind-shear conditions"

INTEGRAL SAFETY SPECTRUM

The *integral flight safety spectrum*, Σ, depicts changes in the situation's safety performance as a whole, and it is constructed according to the following algorithm [1]:

$$(\forall t)\ (t\in[t_*;t^*])\ (\exists\xi(x_k(t)))\ (\xi(x_k(t))\in\{\xi_G,\ \xi_A,\ \xi_R,\ \xi_B,\ \xi_W,\ \ldots\}\ \wedge\ (\xi_B<\xi_R<\xi_A<\xi_G<\xi_W))\ (\xi(t)=max\xi(x_k(t)),\ k=1,\ \ldots,\ p)\ \Rightarrow\ (\xi(t)\in\Sigma\ \wedge\ \Sigma=\xi(t_*)\ ||\ \xi(t_*+\Delta)\ ||\ \ldots\ ||\ \xi(t^*)), \quad (2)$$

where t is time, ξ_i is a safety color code from the safety palette, $i\in${G, A, R, B, W, …}; < is a 'colder than' operation in safety color comparisons; *max* is the operation of selecting the 'hottest' - at a given time instant t - color code $\xi(x_k(t))$; || is the operation of concatenation of successive color-code bars $\xi(t)$ in spectrum Σ; $[t_*;t^*]$ is the analyzed flight time interval, $t_*=t(\mathbf{E}_*)$, $t^*=t(\mathbf{E}^*)$, where $\mathbf{E}_*\equiv\mathbf{E}_1$ and $\mathbf{E}^*\equiv\mathbf{E}_8$ in the example; Δ is the time increment to form the spectrum Σ bar; p is the total number of monitored state variables, p=20.

The meaning of algorithm (2) is as follows. For each time instant t of the examined situation, $t\in[t(\mathbf{E}_*);t(\mathbf{E}^*)]$, a color-coded element that exhibits the 'hottest' color - among the safety colors registered in partial flight safety spectra Σ_k at t - is added to the integral flight safety spectrum bar Σ, k=1, …, p. As a result, at each time instant t integral safety spectrum Σ accounts for the highest degree of violation among all monitored fuzzy constraints $\boldsymbol{C}(x_1)$, …, $\boldsymbol{C}(x_p)$. Therefore, this concept helps represent *safety dynamics* of a flight situation with multiple constraint infringements as a single visual image. This image is intuitively clear and naturally color-coded, and it is based on all available measurements of the system's state vector between $\mathbf{E}_*$ and $\mathbf{E}^*$.

Note. There may be other assumptions and techniques employed to account for safety information stored in Σ_k in Σ. For example, it is possible to rank partial spectra Σ_k in (2) and make some of these spectra unclear ('shadowing') or more important than others, etc.

SITUATION COMPLEXITY BUILD-UP DIAGRAM

The developed technique offers advanced graphic-analytical means to model and represent the overall complexity level of a flight situation. The *situation complexity build-up diagram* is a graphic time-history of the number of penetrations of the 'amber', 'red' and 'black' zones of fuzzy constraints admitted by all monitored state variables, i.e. $\sigma(\xi_A)\cup\sigma(\xi_R)\cup\sigma(\xi_B)$ = $f(t)$. An example of the flight situation complexity build-up diagram for takeoff scenario **S** at Θ_G=16° and γ_G=+22.5° ('flight' $\boldsymbol{F}_{2782}$) is shown in **Fig. 6**.

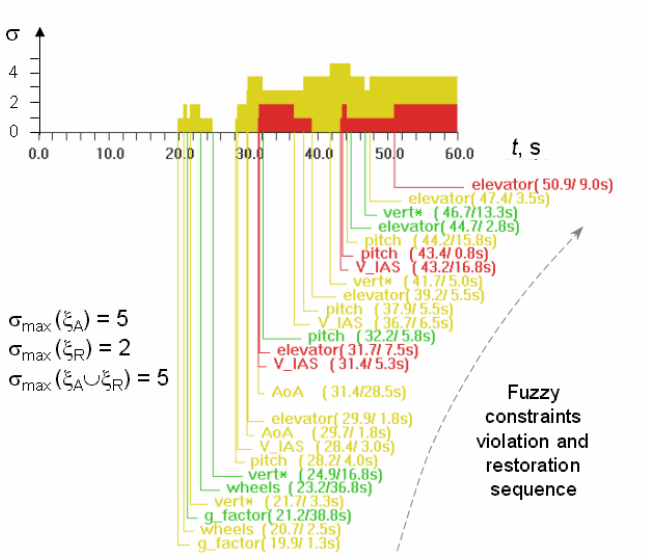

Legend:

σ - number of fuzzy constraint violations (total number of 'visits' of a monitored state variable x to zones ξ_A, ξ_R) at time instant t

Fig. 6: Situation complexity build-up diagram, fuzzy constraint violation and restoration chronology - 'flight' $\boldsymbol{F}_{2782}$: "Normal takeoff, initial climb, Θ_G=16°, γ_G=+22.5°, and 'very strong' wind-shear"

It follows from Fig. 6 figure that *'amber' spikes* normally precede 'red' violations of constraints. These 'spikes'

may serve as visual indicators of accumulating/ approaching danger in flight. Also shown in Fig. 6 is the diagram of *fuzzy flight constraint violation/ restoration chronology and interdependence*. Each message on this diagram has the format: [*variable*] ([*safety color change time*, *s*] / [*duration of a new safety status, s*]s). The message's color corresponds to a new safety status acquired by the system at *t*. The density of vertical hairlines reflects the complexity level of the system state observation task performed by the operator at constraints. Therefore, the developed technique helps study logical mechanisms of cross-coupling violations (and restorations) of flight constraints.

'MACRO-STRUCTURAL' ANALYSIS EXAMPLE

SITUATIONAL TREE

Fig. 7 depicts an axonometric projection of a *situational tree of flight*, $\underline{\boldsymbol{T}}_{130}$, in earth coordinates, $\underline{\boldsymbol{T}}_{130} = \{\boldsymbol{F}_{2682}, \ldots, \boldsymbol{F}_{2811}\}$. Basically, $\underline{\boldsymbol{T}}_{130}$ is a union of 130 'flights'/branches constructed according to scenario **S** (see Fig. 3) under variations/errors of the goal flight path and bank angles, Θ_G and γ_G, during initial climb. The tree's crown coloring scheme corresponds to the integral flight safety spectra of its branches - 'flights' $\boldsymbol{F}_k$. In Fig. 7, code *k* is shown in brown at each branch's end. It follows from the diagram that the situational tree concept can be used, in particular, to compare a set of 'neighboring' non-standard flight cases in desired coordinates. It gives a "bird's eye view" of joint effects of various operating and design factors on the location and safety status of alternative flight trajectories. In addition, selected events from $\Omega(\mathbf{E})$ can be shown attached to the tree's branches as color-coded dots - see the diagram. This feature is particularly useful in flight scenario logic analyses.

Comprehensive situational trees and their graphic representations can be generated under multi-factor conditions in autonomous fast-time simulation experiments using VATES.

OPERATIONAL HYPOTHESIS (TREE'S GENOTYPE)

In order to 'plant' a situational tree, its genotype must be set up to represent a certain *operational hypothesis*, **Γ**, i.e. a desired combination and sequence of the operating/design factors **Φ** selected for examination:

$$\boldsymbol{\Gamma} = \prod_{i=1}^{n}\left[\sum_{k=1}^{m}\boldsymbol{\Phi}^{i}_{k}\right], \qquad (3)$$

where $\boldsymbol{\Phi}^{i}_{k}$ is a *k*-th dependent factor on *i*-th independent level of branching, *i*=1, …, *n*, *k*=1, …*m*; Π is the Cartesian product operation and Σ is the operation of dependent combination of the examined factors. For example, the genotype of the situational tree shown in Fig. 7 implements operational hypothesis $\boldsymbol{\Gamma}(\boldsymbol{\Phi}_1\times\boldsymbol{\Phi}_2\times\boldsymbol{\Phi}_3)$, where $\boldsymbol{\Phi}_1\equiv\Theta_G$, $\boldsymbol{\Phi}_2\equiv\gamma_G$ and $\boldsymbol{\Phi}_3\equiv(W_{xg},W_{zg}=f(t))$ [1]. Values of the first two contributing operating factors, $\boldsymbol{\Phi}_1$ and $\boldsymbol{\Phi}_2$, are combined in the scenarios of $\underline{\boldsymbol{T}}_{130}$ branches according to a Cartesian product rule. The third factor, $\boldsymbol{\Phi}_3$, affects the entire situation. In VATES (v.7), the maximum number of levels of independent branching in a situational tree, *n*, is seven (ref. Fig. 2), and the maximum number of dependent factors combined at each level, *m*, is equal to four.

In addition to (3), special algorithms, which perform functions of growth control and monitoring over a situational tree, are employed to secure a comprehensive yet computationally manageable hypothesis **Γ**. This list includes the following functions: a tree's crown shaping, branch implanting and trimming, crown density and volume monitoring, growth direction control, etc. These algorithms are based on the theory of fractals, *L*-systems [9-11], and incorporate some other methods.

'VIRTUAL FLIGHT SAFETY TEST' EXPERIENCE

The total '*virtual flight [safety test]' experience*, $\Im$, accumulated in some situational tree $\boldsymbol{T}$ is calculated as follows [4]:

$$\Im\,|\,\boldsymbol{T} = \sum_{i=1}^{N(\boldsymbol{T})}\Delta t(\boldsymbol{B}_i)\,, \qquad (4)$$

where $N(\boldsymbol{T})$ is the total number of branches in $\boldsymbol{T}$, and $\Delta t(\boldsymbol{B}_i)$ is the 'length' of branch $\boldsymbol{B}_i$ from the tree's root △ to a leaf ◊ measured in time units, *i*=1, …, $N(\boldsymbol{T})$. In particular, for the situational tree $\underline{\boldsymbol{T}}_{130}$ example depicted in Fig. 7, we have: $\Delta t(\boldsymbol{B}_i)\equiv const$=60 s and $N(\underline{\boldsymbol{T}}_{130})$=130. Thus, $\Im|\underline{\boldsymbol{T}}_{130}\approx 2.17$ hrs.

Note. In metric (4), the length of all parts, including coincident (scenario-wise) parts, of all $N(\boldsymbol{T})$ branches constituting a situational tree is taken into account. This is how a human pilot's flying expertise is rated and compared. However, for the purpose of flight safety analysis and protection in rare multi-factor situations (on higher levels of **Γ**), in addition to $\Im$ it is expedient to introduce a more refined measure of flying expertise, $\Im_N$. It is to account for a *novel flight experience* of an operator (a human pilot or automaton) stored in its 'internal situational tree'. This metric accumulates the duration of only those dissimilar (scenario-wise) parts of $\boldsymbol{B}_i$ that have *n-r*+1, .., *n* factors 'implanted' in them according to the last *r* levels of genotype **Γ**. Parameter *r* is the 'thickness' of an outer, shell-type subset of the situational tree crown. That is, $\Im_N = \Im|\boldsymbol{T} - \Im|\boldsymbol{T}^{n-r}_{\cap}$, where $\boldsymbol{T}^{n-r}_{\cap}$ is a common sub-tree (a non-empty intersection subset) of all $\boldsymbol{B}_i$ with the first *n-r* factor levels, $\boldsymbol{T}^{n-r}_{\cap}\subset\boldsymbol{T}$.

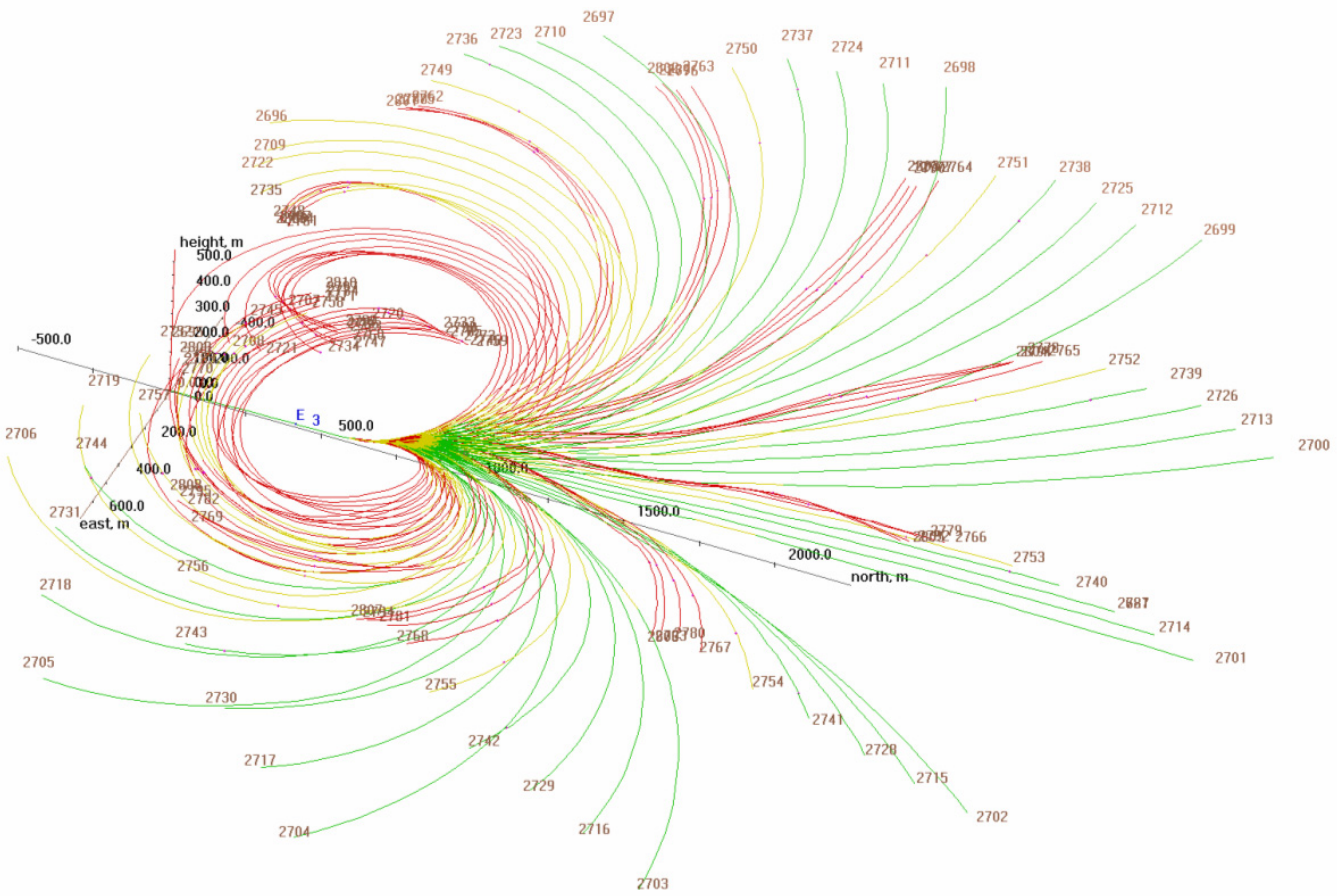

Fig. 7: Situational tree $\underline{\boldsymbol{T}}_{130}$: "Normal takeoff and initial climb. 'Very strong' wind-shear and variations/errors in maintaining Θ_G and γ_G", where $\Theta_G \in \{2^o, \ldots, 20^o\}$, $\gamma_G \in \{-45^o, \ldots, +45^o\}$, $\underline{\boldsymbol{T}}_{130}=\{\boldsymbol{F}_{2682}, \ldots, \boldsymbol{F}_{2811}\}$, $\boldsymbol{\Gamma}(\boldsymbol{\Phi}_1 \times \boldsymbol{\Phi}_2 \times \boldsymbol{\Phi}_3)$ - genotype, $\boldsymbol{\Phi}_1 \equiv \Theta_G$, $\boldsymbol{\Phi}_2 \equiv \gamma_G$, $\boldsymbol{\Phi}_3 \equiv (W_{xg}, W_{zg}=f(t))$

The genotype or operational hypothesis ($\boldsymbol{\Gamma}$) and the virtual flight experience measures ($\mathfrak{I}$, $\mathfrak{I}_N$) of tree $\boldsymbol{T}$ determine, respectively, the *specialization area* and the *maturity/proficiency level* of the situational knowledge base stored in $\boldsymbol{T}$. It is essential that these concepts are physics- and logics-based. In advanced AI backup flight control/safety systems, information on $\boldsymbol{\Gamma}$, $\boldsymbol{T}$, $\mathfrak{I}$, and $\mathfrak{I}_N$ can be used, in particular, for automatic transfer of the control authority to the most competent operator (a human pilot, or automaton) under critical conditions.

TREE'S COMPLEXITY BUILD-UP DIAGRAMS

A family of a *situational tree's complexity build-up diagrams* is shown in **Fig. 8.** These diagrams correspond to a small subset of 'flights', $\{\boldsymbol{F}_{2642}, \ldots, \boldsymbol{F}_{2654}\}$, taken from another situational tree, $\boldsymbol{T}_{130} = \{\boldsymbol{F}_{2551}, \ldots, \boldsymbol{F}_{2680}\}$. The latter has a simpler genotype, $\boldsymbol{\Gamma}(\boldsymbol{\Phi}_1 \times \boldsymbol{\Phi}_2)$, i.e. without the effect of factor $\boldsymbol{\Phi}_3$ - a 'very strong' wind-shear. 'Flights' $\boldsymbol{F}_{2642}, \ldots, \boldsymbol{F}_{2654}$ correspond to non-standard operating conditions at $\Theta_G=+16^o$ and $\gamma_G=var.$ Fig. 8 illustrates the effect of the magnitude and direction of bank on the flight situation complexity and fuzzy constraints violation sequence. It follows from the figure that the flight situation complexity build-up diagrams are sensitive to the direction of the airplane roll - their shapes are different for the left and right bank angles of the same magnitude.

Therefore, the developed technique helps capture even small aerodynamic asymmetries characteristic to the vehicle. These irregularities can be noticed by visually comparing the flight complexity diagrams and safety performance metrics for symmetric left- and right-hand bank maneuvers. Also, the following parameters from the table (see Fig. 8) are helpful to compare for the analyzed 'flights': safety color codes for variables x_k, which exhibit violations of fuzzy constraints $\boldsymbol{C}(x_k)$; relative time (%) when these variables stay inside zones ξ_G, ξ_A and ξ_R; and the overall flight safety index, η [3].

FLIGHT SAFETY INDEX

For any performed (simulated or real) flight situation $\boldsymbol{F}$, its *safety index* can be calculated as follows [3]:

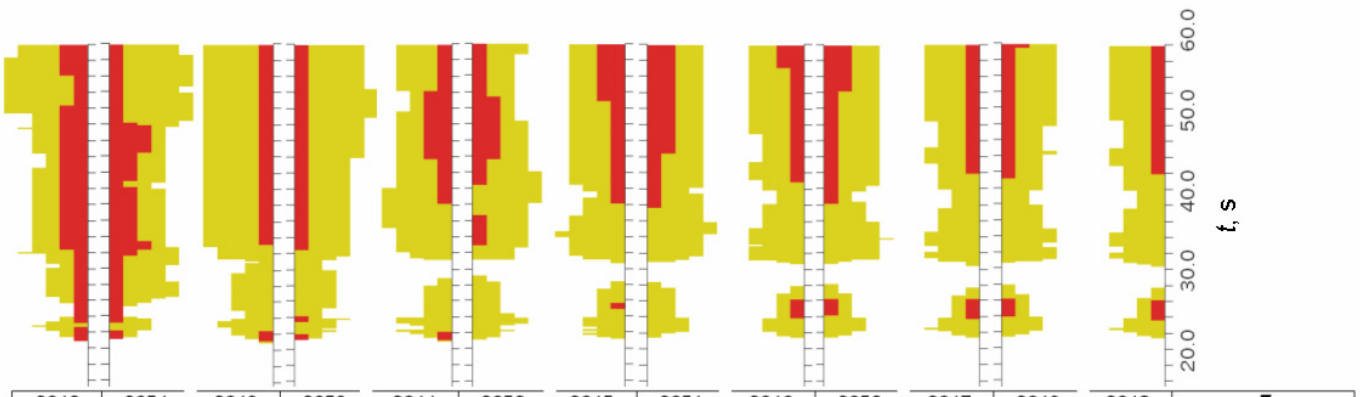

2642	2654	2643	2653	2644	2652	2645	2651	2646	2650	2647	2649	2648	**F**	
-45	+45	-37.5	+37.5	-30	+30	-22.5	+22.5	-15	+15	-7.5	+7.5	0	γ^{o}_{G}	
left	right	left	right	left	right	left	right	left	right	left	right	-	bank	
0.385	0.396	0.517	0.506	0.592	0.586	0.597	0.602	0.615	0.583	0.625	0.619	0.625	η	
	6.0												$C(\underline{n_z})$	Fuzzy constraints violation statistics, Δt_i [%]
55.3	42.1	62.9	64.8	36.5	45.9	18.2	34.6	7.5	15.1		1.9		$C(\delta_e)$	
3.0		2.1	1.3	1.7									$C(\delta_a)$	
88.1	83.6	89.3	1.9 87.4										$C(\gamma)$	
						1.9		5.7	5.0	6.3	5.7	6.3	$C(V_{zg})$	
74.3	7.8	100.	100.	51.9	40.7 59.3	72.7	75.2	62.7	72.7	58.6	61.8	58.6	$C(V_{IAS})$	
100.	100.	100.	100.	99.1	100.	87.3	100.	81.8	85.5	79.3	81.8	80.2	$C(\alpha)$	
		82.4	56.6	73.6	59.1	79.9	80.5	79.9	79.9	79.9	79.9	79.2	$C(\vartheta)$	

Fig. 8: Effect of magnitude and direction of bank on flight situation complexity – a sub-tree from situational tree $\boldsymbol{T}_{130}|\boldsymbol{\Gamma}(\boldsymbol{\Phi}_1\times\boldsymbol{\Phi}_2)$: "Takeoff and initial climb, γ_G=*var*, Θ_G=16°, $\gamma_G\in\{-45^o, \ldots, +45^o\}$", where $\boldsymbol{T}_{130}=\{\boldsymbol{F}_{2551}, \ldots, \boldsymbol{F}_{2680}\}$, $\boldsymbol{\Phi}_1\equiv\Theta_G$, $\boldsymbol{\Phi}_2\equiv\gamma_G$

$$\eta = max\left(0,\ 1-\frac{\Delta t_R + k_A\cdot\Delta t_A + k_B\cdot\Delta t_B}{\Delta t_G + \Delta t_R + \Delta t_A + \Delta t_B}\right), \qquad (5)$$

where Δt_i is the total length (in time units) of all ξ_i-colored zones in all partial safety spectra $\boldsymbol{\Sigma}_k$ of the 'flight', k=1, …, p, $i\in$G, A, R, B}, k_A=0.25 and $k_B=(k_A)^{-1}$ are weight coefficients (an assumption). Index η takes into account the duration of the presence of all monitored state variables x_k near and beyond assigned flight limits. That is, for each variable x_k the flight safety index measures the proximity of its values $x_k(t)$ to fuzzy constraint $\boldsymbol{C}(x_k)$ at ξ_A, ξ_R and ξ_B levels, $t\in[t(\mathbf{E}_\cdot);t(\mathbf{E}^*)]$. Therefore, metric (5) may be viewed as a universal (time-based) measure of the overall system's safety performance in a complex situation with multiple/ overlapping violations of flight constraints.

OPERATING FACTOR EFFECTS

The effect of operating factor Θ_G on the flight situation complexity build-up diagrams, $\sigma(\xi_A)\cup\sigma(\xi_R)=f(t)$, and safety indices, η, of a subset of 'flights' from $\boldsymbol{T}_{130}$ (at Θ_G=*var* and γ_G=-30°) is shown in **Fig. 9** as an example. It can be noticed (see Fig. 9) that the safest (optimum) takeoff scenario performed under $\boldsymbol{\Gamma}(\boldsymbol{\Phi}_1\times\boldsymbol{\Phi}_2)$ conditions corresponds to $\Theta_G\approx7^o$. The 'safest scenario' here is a scenario that secures the largest distance, measured in Θ units, from all monitored constraints, in this case from those ones from variants $\boldsymbol{F}_{2553}$ and $\boldsymbol{F}_{2618}$. Note, however, that the safety index for the optimum scenario (η≈0.98) is slightly lower than its maximum value (η=0.983) recorded for scenario $\boldsymbol{F}_{2566}$ at $\Theta_G=4^o$. It can also be seen that the red zone of fuzzy constraint violations expands quickly along the time axis (from right to left, towards event $\mathbf{E}_3$) when Θ grows above 14°. The intensity of these violations increases too. And again, steady 'red' violations of fuzzy constraints ($\sigma_{max}(\xi_R)$=1…2) are preceded by noticeable 'amber spikes' ($\sigma_{max}(\xi_A)$=2…3) 2-4 s before that violation. For the operator (a pilot or automaton) this relationship may serve as an indicator of a developing danger and as an estimate of the available time reserve.

Thus, flight situation complexity build-up diagrams carry valuable predictive information on the dynamics and intensity of multiple infringements of flight constraints under non-standard conditions.

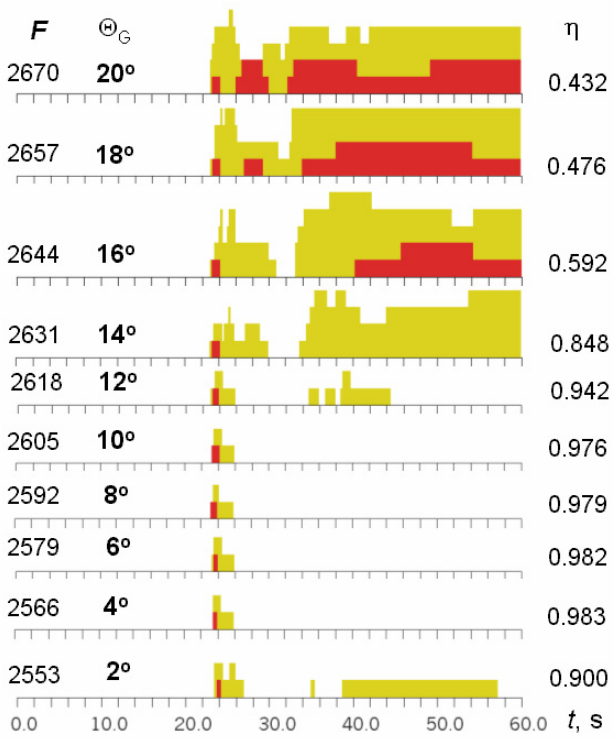

Fig. 9: Situation complexity build-up diagrams - a sub-tree from $\boldsymbol{T}|\boldsymbol{\Gamma}(\boldsymbol{\Phi}_1\times\boldsymbol{\Phi}_2)$: "Takeoff and initial climb, Θ_G=*var*, γ_G=-30°, $\Theta_G\in\{2°, 4°, \ldots, 20°\}$"

SAFETY CAUSE-AND-EFFECT MECHANISMS

The structure of another VATES output format designed to map the *cause-and-effect mechanisms underlying the system's safety performance* is explained in **Fig. 10**. A small subset of 'flights' from $\boldsymbol{T}_{130}$ is presented as an example. This format combines the following safety-critical information items: a tree's integral flight safety spectra, examined operating factors and their current values, flight safety indices, fuzzy constraints violation statistics, and key flight events linked to the common time scale of the flight safety spectra. The use of this 'knowledge map' for causal analysis of an aircraft's flight safety performance is described below.

CAUSAL ANALYSIS OF SAFETY PERFORMANCE

An example of the cause-and-effect analysis of a tree's integral safety spectra is given in **Fig. 11**, the right-hand diagram. The goals are as follows: (1) reveal the overall safety topology of a family of non-standard takeoff scenarios exemplified in $\boldsymbol{T}_{130}$, and (2) show correlations between (a) the examined values of operating factors $\boldsymbol{\Phi}_1$ and $\boldsymbol{\Phi}_2$ and (b) the level of violations of fuzzy constraints and flight safety indices. Digits **1** to **9** denote nine characteristic 'cases' (groups of 'flights') that have different cause-and-effect relationships. On this diagram, case **1** 'flights' stand for periodic, i.e. observed from 'flight' to 'flight', 'red' spikes occurred due to extreme bank angle, accompanied by escalating violations of the elevator constraint as the flight path angle increases. Case **2** 'flights' relate to multiple or coupled infringements of constraints (V_{IAS}-δ_e, and some other constraint pairs) or these constraints proximity (α-ϑ, and other combinations) observed at very large (+16°…+18°) flight path angles. Case **3** 'flights' exhibit 'red' spikes, observed from 'flight' to 'flight', due to reaching elevator limits at $\Theta\approx$+14°…+16° and $|\gamma|\approx$37.5°. Case **4** 'flights' proceed in close proximity to 'low V_{IAS}' and 'large ϑ' constraints (the 'amber' zone) at $\Theta\approx$+14°. Case **5** 'flights' demonstrate periodic, from 'flight' to 'flight', 'red' spikes occurred due to the violation of a bank angle constraint. Case **6** scenarios exhibit 'amber' spikes due to proximity of the system state to bank and/or airspeed constraints. Case **7** variants show safe, optimal and sub-optimal, 'green' performance. Case **8** flights have characteristic 'amber' spikes, observed from 'flight' to 'flight', due to proximity to a 'large γ' constraint. Finally, case **9** 'flights' demonstrate the dominance of 'amber' color due to close proximity to an 'insufficient climb rate' constraint.

Therefore, key cause-and-effect relationships between examined operating/design factors and the system's safety performance metrics under non-standard conditions can be identified. The technique helps determine critical combinations and values of the examined factors, split the tested domain of complex flight scenarios on to characteristic subsets. Then a list of the constraints, which are most likely to be infringed, is derived automatically together with key contributing factors for each characteristic subset of flights.

SAFETY TOPOLOGY COMPARISON OF TWO TREES

An ordered family of the integral safety spectra of 'flights' constituting a situational tree represents its *safety topology*. A comparison of the safety topologies of two trees, $\boldsymbol{T}_{130}|\boldsymbol{\Gamma}(\boldsymbol{\Phi}_1\times\boldsymbol{\Phi}_2)$ and $\underline{\boldsymbol{T}}_{130}|\ \boldsymbol{\Gamma}(\boldsymbol{\Phi}_1\times\boldsymbol{\Phi}_2+\boldsymbol{\Phi}_3)$, is shown in Fig. 11 as an example. Note that any two 'flights', from $\boldsymbol{T}_{130}$ and $\underline{\boldsymbol{T}}_{130}$ respectively, with integral safety spectrum bars located at the same level on the diagram, have equal values of operating factors $\boldsymbol{\Phi}_1$ and $\boldsymbol{\Phi}_2$. For example, 'flights' $\boldsymbol{F}_{2651}$ and $\boldsymbol{F}_{2782}$ correspond to Θ_G=16° and γ_G=22.5°, where $\boldsymbol{F}_{2651}\in\boldsymbol{T}_{130}$ and $\boldsymbol{F}_{2782}\in\underline{\boldsymbol{T}}_{130}$.

From this comparison it can be concluded, in particular, that if a 'very strong' wind-shear profile ($\boldsymbol{\Phi}_3$) is added ($\underline{\boldsymbol{T}}_{130}$), then the system's safety performance is likely to change substantially at very small (Θ_G=2°) and at very large ($\Theta_G\geq$14°) flight path angles. The introduced wind-shear results in a fatal outcome of the takeoff scenarios performed at small flight path angle (Θ_G=2°) – see 'black' safety spectra of 'flights' $\boldsymbol{F}_{2682}$, …, $\boldsymbol{F}_{2694}$ (the left-hand diagram in Fig. 11).

It also follows from the diagram that in the scenarios under a 'very strong' wind-shear condition with Θ_G=14° and $|\gamma_G|\in$[30°;37.5°] it is possible to reduce a sharp loss

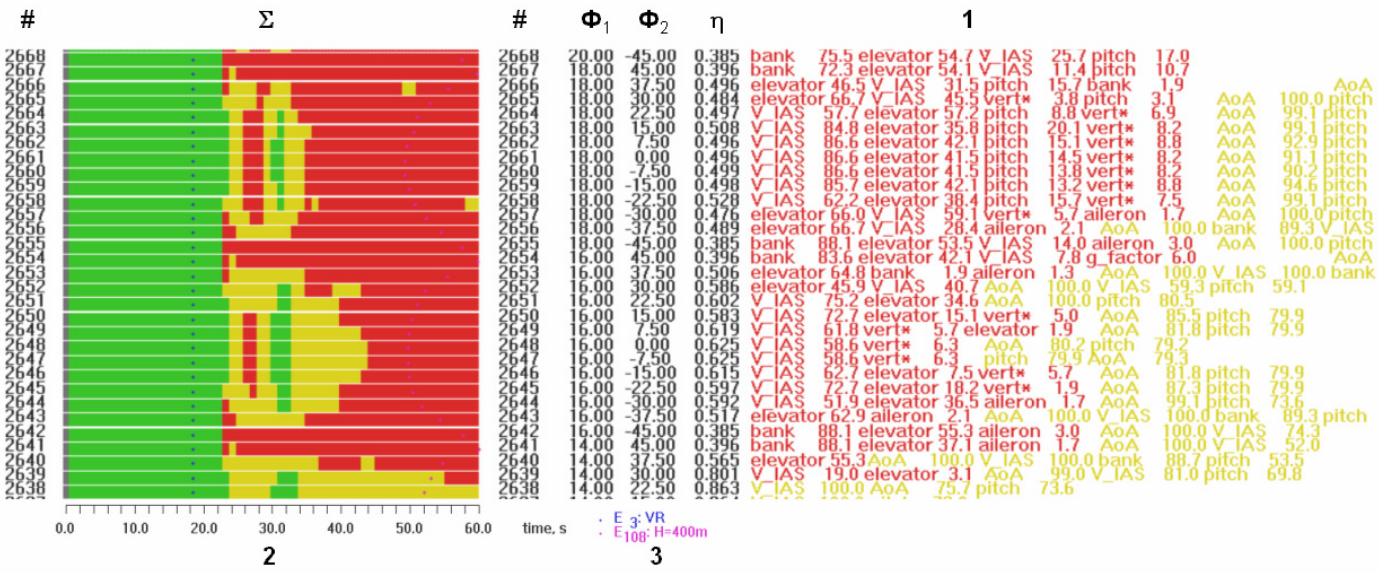

Legend:

- code of "flight" from $\boldsymbol{T}_{130}$; **Σ** - integral flight safety spectrum; $\boldsymbol{\Phi}_1$ – value of operating factor Θ_G; $\boldsymbol{\Phi}_2$ - value of operating factor γ_G; **η** - flight safety index; **1** – messages on fuzzy constraint violations; **2** – common time scale of 'flights', s; **3** – characteristic events depicted on integral safety spectra ($\mathbf{E}_3$ and $\mathbf{E}_{108}\equiv\mathbf{E}_{12}$ - ref. Fig. 3)

Fig. 10: Integral flight safety spectra, examined operating factors, flight safety indices and fuzzy constraints violation statistics for a subset of "flights" from $\boldsymbol{T}_{130}$

of the vehicle's kinetic energy. This can be achieved by changing the aircraft heading angle, i.e. by applying a medium commanded bank angle $|\gamma_G|$ in initial climb. However, this method is valid if and only if a prevailing wind-shear direction is known. These improved takeoff options exhibit amber-color coded split-'c' patterns across their spectra $\Sigma(\mathbf{F}_i)$ - ref. $\Sigma(\mathbf{F}_i)$ for 'flights' {$\boldsymbol{F}_{2761}$, $\boldsymbol{F}_{2762}$, $\boldsymbol{F}_{2769}$, …, $\boldsymbol{F}_{2771}$, $\boldsymbol{F}_{2774}$, $\boldsymbol{F}_{2784}$}. Thus, the examined 'very strong' wind-shear profile can theoretically improve the integral safety spectra of several non-standard climb options from $\underline{\boldsymbol{T}}_{130}$ compared to hypothesis $\boldsymbol{\Gamma}(\boldsymbol{\Phi}_1\times\boldsymbol{\Phi}_2)$ with no wind at takeoff. Note also that the optimal flight path angles for $\boldsymbol{T}_{130}$ and $\underline{\boldsymbol{T}}_{130}$ are different: $\Theta_{opt}\approx 8^o$ and $\Theta_{opt}\approx 6.5^o$, respectively. Finally, in the wind-shear scenarios ($\underline{\boldsymbol{T}}_{130}$) the vehicle is experiencing a strong head-wind effect during ground-roll. As a result, event $\mathbf{E}_3$: "*VR* achieved" in $\underline{\boldsymbol{T}}_{130}$ is recognized earlier: $t(\mathbf{E}_3)$=16.3 s for $\underline{\boldsymbol{T}}_{130}$ and $t(\mathbf{E}_3)$=18.65 s for $\boldsymbol{T}_{130}$. Thus, the integral safety spectrum concept and situational tree concepts enable a quick "bird's eye view" analysis and comparison of the overall safety topology of a complex flight domain at constraints under various operational hypotheses.

ANOTHER TREE GENOTYPE EXAMPLE

Fig. 12 depicts flight safety topology for another tree's genotype $\boldsymbol{\Gamma}(\boldsymbol{\Phi}_4\times\boldsymbol{\Phi}_5)$: "Takeoff with left-hand engine out at airspeed V_{LEO} ($\boldsymbol{\Phi}_4$) and cross-wind velocity W_{zg} ($\boldsymbol{\Phi}_5$)", where $\Omega(\boldsymbol{\Phi}_4)$={115, …, 205} [km/h] and $\Omega(\boldsymbol{\Phi}_5)$={-18, …, +18} [m/s]. This figure demonstrates, in particular, joint effects of two operating factors, V_{LEO} and W_{zg}, on the system's safety performance and on the position of selected key events ($\mathbf{E}_3$, $\mathbf{E}_7$). It also helps identify critical pairs of (V_{LEO}, W_{zg}) values and determine the location and shape of the *'anomalies'* in the safety topology of this particular tree. These are prohibitively dangerous subsets of 'flights' with prevailing ξ_R and ξ_B levels in their safety spectra.

VFT&E TECHNIQUE CAPABILITIES

The presented safety knowledge-mapping formats and analysis examples demonstrate the following *capabilities of the VFT&E technique*:

- fast-time autonomous simulation and a "bird's eye view" type exploration of the safety topology of a complex (multi-factor) flight situation domain,
- numeric assessment of the system's safety performance for a broad range of anticipated flight conditions,
- identification of potentially dangerous combinations of heterogeneous operating/design factors and prohibited flight scenarios,
- identification of cause-and-effect relationships between examined operating/design factors and the system's safety performance metrics under non-standard conditions,
- detection of potentially unsafe anomalies in the system behavior, their shape and dynamics, and
- simulation-based search of optimal and sub-optimal (safety-wise) values of flight scenario parameters.

Fig. 11: Causal analysis of situational tree $\boldsymbol{T}_{130}$ integral safety spectra (right-hand diagram; **j** – characteristic subset of 'flights', **j=1**, **2**, …, **9**). Safety topology comparison of two trees: $\underline{\boldsymbol{T}}_{130}|\boldsymbol{\Gamma}(\boldsymbol{\Phi}_1\times\boldsymbol{\Phi}_2\times\boldsymbol{\Phi}_3)$ and $\boldsymbol{T}_{130}|\boldsymbol{\Gamma}(\boldsymbol{\Phi}_1\times\boldsymbol{\Phi}_2)$

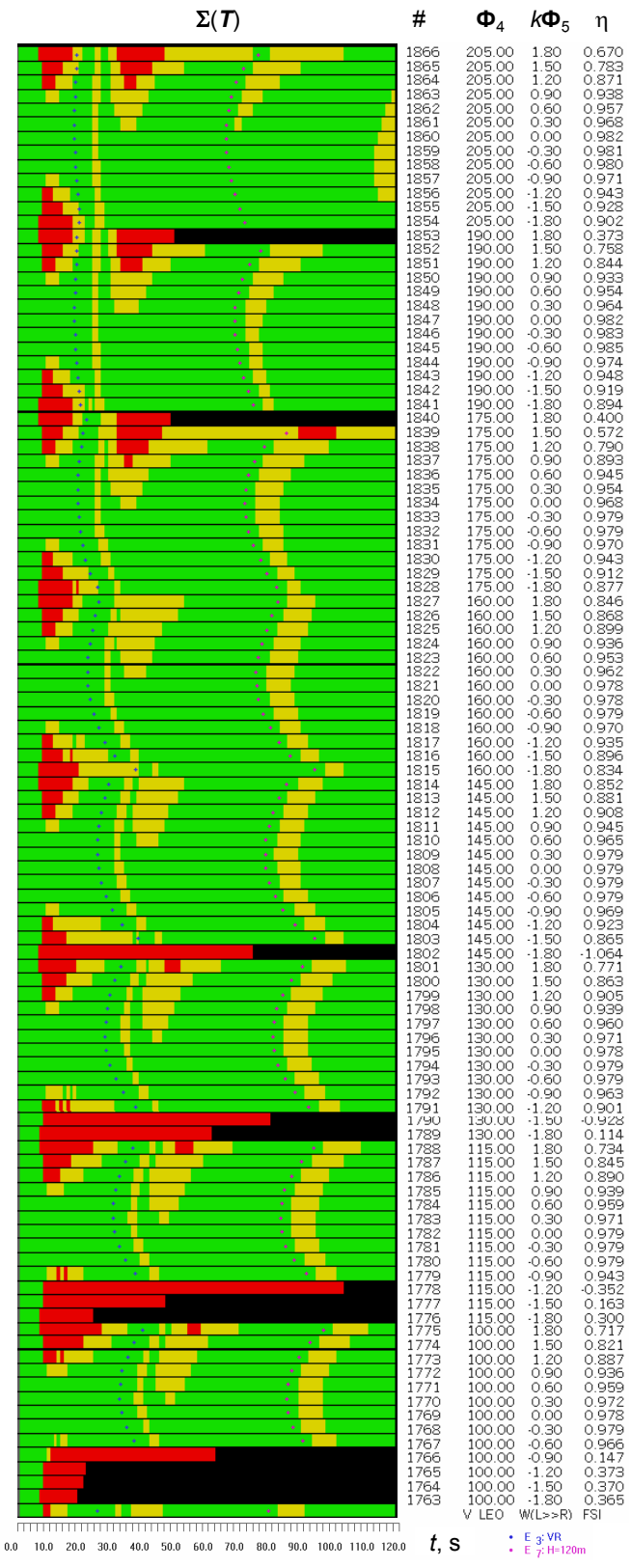

Fig. 12: Flight safety topology of situational tree $T|\Gamma(\Phi_4\times\Phi_5)$: "Continued takeoff, left-hand engine out at V_{LEO} ($V_{LEO}\equiv\Phi_4$) in ground-roll and crosswind ($W_{zg}\equiv\Phi_5$)", $\Omega(\Phi_4)$ = {100, …, 205} km/h, $\Omega(\Phi_5)$={-18, …, +18} m/s, k=10^{-1}

This analytical potential is employed below to predict the system's overall safety performance under multi-factor conditions using the concepts of flight safety category and safety window.

SYSTEM SAFETY PREDICTION

SAFETY CATEGORIES

The following *five flight [situation] safety categories* are defined in **Table 1** [3]: Safe (**I**), Conditionally Safe (**II**), Potentially Unsafe (**III**), Dangerous, or Prohibited (**IV**), and Catastrophic ('chain reaction') type (**V**) situations. This generic 'safety measurement scale' is particularly useful for ranking various flight alternatives according to their overall safety status based on the information stored in their integral safety spectra. For example, a partitioning of the set of non-standard situations constituting T_{130} onto equal-safety clusters in accordance with their overall flight safety performance is summarized in **Table 2**.

Table 1: Definition of flight safety categories

Flight safety category			Flight situation classification criterion
Color	Code	Name	
	I	Safe	The system states mainly reside in the 'green' zone. As a maximum, the system state may stay, for a *short time*, in close proximity to flight constraints, i.e. inside the 'amber' zone, but must leave it by the end of the situation
	II-a	Conditionally Safe – a	As a maximum, the system state may stay, for a *medium time* (**a**) or for a *long time* (**b**), in close proximity to flight constraints, i.e. inside the 'amber' zone
	II-b	Conditionally Safe – b	
	III	Potentially Unsafe	As a maximum, the system state may violate flight constraints, i.e. enter the 'red' zone, for a *short or medium time*, but must leave it by the end of the situation
	IV	Dangerous (Prohibited)	As a maximum, the system state stays beyond flight constraints, i.e. inside the 'red' zone, for a *long time* or till the end of the situation
	V	Catastrophic ('Chain Reaction')	There is at least one (a *short time*) occurrence of a 'black' violation of a flight constraint

Table 2: Partitioning of the tree T_{130} flight situations according to their safety performance

Membership Category	'Flight' ## (130 'flights' in total)	%
Safe (**I**)	2566-2574, 2579-2587, 2592-2600, 2605-2613, 2618-2625 (44 'flights')	33.8
Conditionally	2552-2562, 2565, 2575, 2578, 2588,	23.1

Safe (**II-b**)	2591, 2601, 2604, 2614, 2617, 2626, 2627, 2631-2638 (30 'flights')	
Dangerous, or Prohibited (**IV**)	2551, 2563, 2564, 2576-2577, 2589-2590, 2602-2603, 2615-2616, 2628-2630, 2639-2680 (56 'flights')	43.1

Note. The meaning of fuzzy terms 'short time', medium time', and 'long time' from Table 1 is intuitively clear. However, it can be formalized in computer algorithms to avoid misinterpretation.

CLASSIFICATION ALGORITHM

A generic algorithm for automatic, batch-type classification of large sets of non-standard flight situations has been developed using the five safety categories defined in Table 1. In particular, it follows from Table 2 that 'flights' rated as Category **III** or Category **V** situations are absent in tree $\boldsymbol{T}_{130}$. All other examined situations belong to Safe (**I**), Conditionally Safe (**II-b**) and Dangerous (Prohibited) (**IV**) flight situation subsets. **Fig. 13** depicts a sector diagram showing a *distribution of the tree's 'flights' due to their safety performance*. This type of diagram is an essential predictive part of the flight safety indicator concept proposed in [1]. An empty subset of 'flights' for Category **III** may indicate that the aerodynamic layout of this airplane or/and flight scenario **S** contain shortcomings, which can trigger, under certain circumstances, an abrupt transition of the system from safe states to unsafe ones. A further refinement of the tree's genotype is possibly needed to explore in depth this boundary sub-domain of the system states and transitions.

Therefore, the concepts of flight safety category and integral flight safety spectrum help automate the task of partitioning of a large number of non-standard situations generated in VATES-based simulation experiments onto equal-safety clusters. This algorithm can also be applied to assess safety of flights recorded in manned simulation and operation. The proposed sector diagram concept can be used to dynamically depict a distribution of a subset of 'flights' due to their safety status in advanced onboard AI displays.

SAFETY WINDOW

Fig. 13 illustrates a so called *'flight safety [performance] window'* - an integral visual knowledge map of safe, prohibited and interim flight modes. It is based on the 'performance window' concept proposed by NASA [6]. In the presented study, that original concept has been reworked and implemented on computer [4]. In particular, in addition to the two main - 'green' (ξ_G) and 'red' (ξ_R) - zones, 'amber' (ξ_A), 'black' (ξ_B) and 'white' (ξ_W) zones have been added. A technique has also been developed to link the expanded palette to the five flight safety categories (ref. Table 1). The resulting safety window can be depicted as a 2-, 3-, or 4-D 'virtual reality' image using respectively two, three, or four key, flight-phase dependent, system state variables. The time variable *t* can be added to a safety window as an independent variable thus enabling its real- or fast-time predictive capability. At present, 2-D flight safety windows are constructed automatically with the help of the VATES tool (v.7) based on the formalized criteria introduced in Table 1 and a tree's safety data.

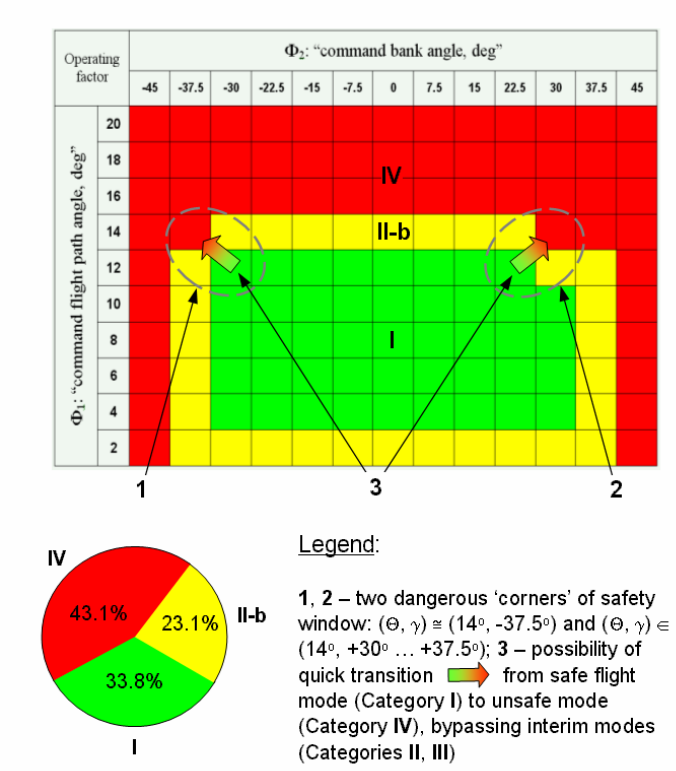

Fig. 13: Distribution of 'flights' due to overall safety status, safety [performance] window for situational tree $\boldsymbol{T}_{130}|\boldsymbol{\Gamma}(\boldsymbol{\Phi}_1\times\boldsymbol{\Phi}_2)$

Shown in Fig. 13 is a safety window constructed automatically in coordinates (Θ_G,γ_G) for an advanced commuter airplane using tree's $\boldsymbol{T}_{130}|\boldsymbol{\Gamma}(\boldsymbol{\Phi}_1\times\boldsymbol{\Phi}_2)$ data. Digits ***1***, ***2*** denote two *potentially unsafe 'corners'* of the safety window that correspond to $(\Theta,\gamma)\cong(14^o, -37.5^o)$ and $(\Theta,\gamma)\in(14^o, +30^o\ldots+37.5^o)$, respectively. At these 'corners', quick transitions ***3*** of the system states are possible from a safe sub-domain to a dangerous one (**I→IV**), bypassing interim Categories **II**, **III**. Further uncontained transitions **IV→V**, i.e. a 'chain reaction' type developments, are not excluded. Therefore, the safety window concept is a carrier of important predictive physics-based information on safe, marginal, unsafe, potentially catastrophic and unknown flight and control modes of an aircraft under non-standard conditions using key state variables.

PILOTING RECOMMENDATIONS

Table 3 contains recommendations on a safe flight control scenario based on the situational tree $\boldsymbol{T}_{130}$ data, i.e. for operational hypothesis $\boldsymbol{\Gamma}(\boldsymbol{\Phi}_1\times\boldsymbol{\Phi}_2)$: "Normal takeoff

and initial climb, benign weather conditions, *mass=xx* tons, C.G.=*xx* %, *flaps=xx* deg".

Table 3: Example of piloting recommendations - takeoff and initial climb

Flight control scenario quality (safety category)	**Goal state ('safety window') variables and their value pairs**	
	Flight path angle, deg	Bank angle, deg
Optimum, window's center, i.e. desirable (**I**)	8	0
Sub-optimum, yet 'green' variants, i.e. acceptable (**I**)	4 … 10 12	-30 … +30 -30 … +22.5
At the edge of safe flying, i.e. marginally acceptable (**II-b**)	2 4…12 12 14	-37.5 … +37.5 -37.5, or +37.5 +30 -30…+22.5
Dangerous, i.e. prohibited, unacceptable (**IV**)	Any <u>14</u> <u>14</u> 16 … 20	-45, or +45 <u>-37.5</u> <u>+30 … +37.5</u> Any

<u>Note</u>: the underlined parameters correspond to the two dangerous 'corners', ***1*** and ***2***, of the safety window shown in Fig. 13.

In particular, it follows from Fig. 13 and Table 3 that the operator (a human pilot or automaton) must exercise enhanced attention and apply accurate piloting techniques if flight proceeds close to 'corners' ***1***, ***2***. An asymmetry observed in the (Θ,γ) safety window along the bank angle coordinate at these 'corners' is due to a turboprop engine's side-wash effect, which is characteristic to the aerodynamic layout of the tested airplane. Therefore, the developed technique accounts for specific aerodynamic and control properties of an aircraft on the level of piloting instructions.

CONCLUSION

The developed autonomous situational model of the 'pilot (automaton) – aircraft – operational environment' system behavior offers an affordable and powerful source of up-front information on the system's safety performance in complex (multi-factor) flight situations. The model can be used to thoroughly examine, both in-breadth and in-depth, the borders of an aircraft's flight envelope under non-standard operating conditions. The goal is to help detect potentially unsafe anomalies in the system behavior and their underlying cause-and-effect mechanisms in advance.

The virtual flight test and evaluation technique complements physical testing and manned simulations in advanced flight safety studies. In many multi-factor cases, which are difficult to construct or unsafe/costly to examine, the model is the only source of knowledge about the future system behavior and safety performance. It enables a safety expert to explore automatically a large number of realistic operational scenarios in autonomous fast-time simulation experiments on a standard PC [4, 5]. In this process, piloting or programming skills are not required. The technique is particularly efficient when a quick comparative safety/performance study of several design alternatives of a future vehicle is required under realistic operational scenarios. Reconstruction of multi-factor accident situations and systematic, 'what-if' analysis of their 'neighborhood' under uncertainty is another proven application area [1].

Finally, the system model, its methodology and implementation tool demonstrate a potential as an integral research framework for prototyping knowledge base and decision-making mechanism components for advanced AI-based flight safety protection systems [2]. The latter include 'future looking onboard safety radars', built-in intelligent systems for backup/overriding safety control of aircraft in emergencies, flight control in unmanned (autonomous) single- and multi-vehicle systems, self-organizing conflict resolution/prevention in congested free-flight air space, etc.

However, in order to obtain reliable results from the system model it is mandatory to have a complete 'parametric definition' of a project/vehicle under examination. This database must encapsulate a sub-domain of the flight and control modes of interest.

ACKNOWLEDGMENTS

The author wishes to thank Prof. Daniel Schrage and Dr. Daniel DeLaurentis, Georgia Institute of Technology, and Dr. Bernd Chudoba, University of Oklahoma, for multi-aspect help and useful discussions on this research topic.

REFERENCES

1. Burdun, I.Y. "The Intelligent Situational Awareness And Forecasting Environment (The S.A.F.E. Concept): A Case Study" (Paper #981223), Proc. of the SAE Advances in Flight Safety Conference and Exhibition, April 6-8, 1998, Daytona Beach, FL, USA (P-321), AIAA-SAE, 1998, pp. 131-144.

2. Burdun, I.Y., Parfentyev, O.M. "Fuzzy Situational Tree-Networks for Intelligent Flight Support", Int. Journal of Engineering Applications of Artificial Intelligence (EAAI), 12 (1999), pp. 523-541.

3. Burdun, I.Y. "Studying Physics and Logics of Complex Flight Situation Domains by Means of VATES Modeling and Simulation Tool", 2nd Science and Technology Conference "Flight Simulation Technologies and Pilot Training: New Approaches and Goals", TsAGI, 24-25 April 2003, Zhoukovsky, Moscow Region, Russia, 2003, 11 pages (in Russian).

4. Burdun, I.Y., and Parfentyev, O.M. "Analysis of Aerobatic Flight Safety Using Autonomous Modeling and Simulation' (Paper #2000-01-2100), Proc. of the 2000 Advances in Aviation Safety Conference, April 11-13, 2000, Daytona Beach, FL, USA (P-355), SAE, 2000, pp. 75-92.

5. Burdun, I.Y., and Mavris, D.N. “A Technique for Testing and Evaluation of Aircraft Flight Performance in Early Design Phases” (Paper #975541), Proc. of the World Aviation Congress (WAC'97), Anaheim, October 1997, CA, USA, AIAA-SAE, 1997, 13 pages.

6. Schrage, D.P., Calise, A.J., Burdun, I.Y., Pritchett, A., and Rysdyk, R.T. “An Integrated Knowledge-Based Approach to Improving Aircraft Safety”, White Paper, School of Aerospace Engineering, Georgia Institute of Technology, USA, October 1998, 20 pages.

7. Bellman, R.E., and Zadeh, L.A. “Decision-Making in a Fuzzy Environment”, NASA Contractor Report, NASA CR-1594, 1970.

8. Burdun, I.Y. “Introduction to Onboard AI for Flight Safety Enhancement”, Lecture Course Notes (Chapters 4-7), Issue 2, Novosibirsk, Russia, 2001, 57 pages (in Russian).

9. Mandelbrot, B.B., “The Fractal Geometry of Nature”, W.H.Freeman, San-Francisco, 1982.

10. Prusinkiewicz, P., and Lindenmayer, A., “The Algorithmic Beauty of Plants”. Springer-Verlag, New York, 1990.

11. Prusinkiewicz, P., Hammel, M., Měch, R., Hanan, J., “The Algorithmic Beauty of Plants”. From: "Artificial Life for Graphics, Animation, and Virtual Reality". Vol. 7, SIGGRAPH '95 Course Notes, pp. 1-1-1-38, ACM Press, 1995.

CONTACT

Dr. Ivan Y. Burdun

[obsolete affiliation and contact information removed]

E-mail: ivan.burdun@mail.ru

DEFINITIONS, ACRONYMS, ABBREVIATIONS

□	Flight process type, □∈{**D**, **B**, **F**, **T**, **P**, **O**, **W**, **L**, **R**, **I**, **Y**, …}
●	‘Bud’-type system state
△	‘Root’-type system state
◊	‘Leaf’-type system state
○	Reference type state
I	‘Safe’ Category flight situations
II	‘Conditionally Safe’ Category flight situations
III	‘Potentially Unsafe’ Category flight situations
IV	‘Dangerous, or Prohibited’ Category flight situations
V	‘Catastrophic (‘Chain Reaction’ Type)’ Category flight situations
130, 2682	Respectively, situational tree code and ‘flight’ code (examples)
#	‘Flight’ code/number
∧	‘And’ (&) logical link
<	‘Is-colder-than’ operation (in two safety colors comparison)
|	In X|Y: X is a property of Y
||	Concatenation operation for safety colors
∪	Set union operation
→	In X→Y: system state transition from Category X to Category Y; X,Y∈{**I**, **II**, …, **V**}
{*a*, *b*, *c*, *d*}	Characteristic points of a fuzzy set-constraint carrier
A	Data flow containing a flight situation scenario
B	Branch (‘flight’) in a situational tree
$\boldsymbol{B}_{-1}$	Parent branch
$\boldsymbol{B}_0$	Tree’s trunk (main, or baseline branch)
$\boldsymbol{B}_n$	Branch of *n*-th level, *n*=1, 2, …
B	‘On-board system function’ type process
B	Data flow containing a 'parametric definition' of a vehicle/project
C	Fuzzy constraint concept (L.A.Zadeh)
$\boldsymbol{C}(x_k)$	Fuzzy constraint for state variable x_k
D	‘Flight dynamics’ type process
E, E	East coordinate
E	Flight event
$\mathbf{E}_*$	Start event
$\mathbf{E}^*$	Stop event
$\dot{E}$	East velocity
f(t)	Function of time *t*
F	‘Flight’ (modeling and simulation experiment output data file)
$\boldsymbol{F}_k$	*k*-th ‘flight’ in a situational tree
F	‘On-board system failure’ type process
H	Flight altitude
I	‘Aircraft surface icing’ type process
k	Ordinal number of a ‘flight’ in a situational tree
k_A	Weight coefficient to account for the duration of zone ξ_A
k_B	Weight coefficient to account for the duration of zone ξ_B
k_{LG}	Wheels position variable, $k_{LG}\in[0;1]$
L	‘Atmospheric turbulence’ type process
m	Maximum number of dependent operating factors combined on each level in a tree
n	Maximum number of independent branching levels in a tree
n_z	Normal load factor
N	North coordinate
$N(\boldsymbol{T})$	Total number of branches in tree ***T***
O	‘’System state observer’ type process
p	Number of monitored state variables (checked constraints)
P	‘Control procedure’ type process
R	‘Rain’ type process
r	'Thickness' of a shell-type subset of novel multi-factor situations
S	Flight [situation] scenario
T, $\underline{\boldsymbol{T}}$	Situational tree of ‘flights’
$\boldsymbol{T}^{n-r}_{\cap}$	Common sub-tree (a non-empty intersection subset) of $\boldsymbol{B}_i$ with the first *n-r* factor levels
T	‘Piloting task’ type process
t_*, t^*	Respectively, start and stop time of a flight situation
t	Flight time
$t(\mathbf{E}_i)$	Time of recognition of event $\mathbf{E}_i$
$t(\mathbf{E}_*)$	Time of recognition of start event $\mathbf{E}_*$
$t(\mathbf{E}^*)$	Time of recognition of stop event $\mathbf{E}^*$
V_{IAS}	Indicated air speed
V_{LEO}	Left engine out speed
V_{zg}	Vertical speed
W	‘Wind’ type process
W_{xg}	Horizontal velocity component of a wind-shear profile

W_{zg}	Vertical velocity component of a wind-shear profile
x	Monitored state variable
x_k	Monitored state variable #k, k=1, …, p
$x_k(t)$	Numeric value of variable x_k at time instant t
$\mathbf{Y}$	'Runway surface condition' type process
$\mathbf{\Gamma}$	Operational hypothesis, or genotype, of a situational tree
α	Angle of attack
β	Sideslip angle
γ	Bank angle
γ_G	Goal (commanded) bank angle
μ	Membership function of a fuzzy set
$\mu_{\boldsymbol{C}}(x)$	Membership function (L.A.Zadeh) of fuzzy constraint $\boldsymbol{C}$ for system state variable x
η	Flight safety index
ξ	Flight safety color
ξ_G	'Green' safety color ('norm')
ξ_A	'Amber' safety color ('attention')
ξ_R	'Red' safety color ('danger')
ξ_B	'Black' safety color ('fatal')
ξ_W	'Gray'/'white' safety color ('unknown')
$\{\xi_G, \xi_A, \xi_R, \xi_B, \xi_W, \ldots\}$	Flight safety palette
$\xi(t)$	Safety color-code bar at time instant t
σ	Flight situation complexity index
$\sigma(\xi_i)$	Number of penetrations of zone ξ_i of a fuzzy constraint by flight variables
$\sigma_{max}(\xi_i)$	Maximum number of penetrations of zone ξ_i of a fuzzy constraint by flight variables
δ_a	Aileron position
δ_e	Elevator position
δ_r	Rudder position
δ_F	Flaps position
Δ	Time increment in the flight safety spectrum formation algorithm [3, 4]
$\Delta t(\boldsymbol{B}_i)$	Branch 'length' in time units
Δt_i	Total length (in time units) of all ξ_i-colored zones in partial safety spectra, $i \in$ {G, A, R, B, W, …}
ϑ	Pitch angle
Θ	Flight path angle
Θ_G	Goal (commanded) flight path angle
Θ_{opt}	Optimum ('maximum safety') value of the flight path angle
$\mathbf{\Pi}$	Flight process
Π	Cartesian product operation
$\Im\|\boldsymbol{T}$	Total 'virtual' flight experience accumulated in situational tree $\boldsymbol{T}$
$\Im_N\|\boldsymbol{T}$	Novel 'virtual' flight experience accumulated in situational tree $\boldsymbol{T}$
$\mathbf{\Phi}$	Operating/design factor
$\mathbf{\Phi}^i_k$	k-th dependent operating or design factor on i-th independent level
$\mathbf{\Phi}_1$	Operating factor #1 "Commanded flight path angle"
$\mathbf{\Phi}_2$	Operating factor #2 "Commanded bank angle"
$\mathbf{\Phi}_3$	Operating factor #3 "Wind-shear profile recorded in a flight accident"
$\mathbf{\Phi}_4$	Operating factor #4 "Left-hand engine out airspeed"
$\mathbf{\Phi}_5$	Operating factor #5 "Crosswind velocity"
$\mathbf{\Gamma}(\mathbf{\Phi}_1\times\mathbf{\Phi}_2)$	Operational hypothesis (Cartesian product of factors $\mathbf{\Phi}_1$and $\mathbf{\Phi}_2$)
$\mathbf{\Gamma}(\mathbf{\Phi}_1\times\mathbf{\Phi}_2\times\mathbf{\Phi}_3)$	Operational hypothesis $\mathbf{\Phi}_1\times\mathbf{\Phi}_2\times\mathbf{\Phi}_3$
$\mathbf{\Gamma}(\mathbf{\Phi}_4\times\mathbf{\Phi}_5)$	Operational hypothesis $\mathbf{\Phi}_4\times\mathbf{\Phi}_5$
Σ	Operation of dependent combination of factors on some level in a situational tree
$\mathbf{\Sigma}_k$	Partial flight safety spectrum
$\mathbf{\Sigma}$	Integral flight safety spectrum
$\Omega(\mathbf{E})$	Calendar of flight events
$\Omega(\mathbf{\Pi})$	United list of flight processes
$\Omega(\square)$	Subset of $\square$-type processes
`aileron`	Identifier of the "ailerons deflection" variable
`AoA`	Identifier of the "angle of attack" variable
`bank`	Identifier of the "bank angle" variable
`east`	Identifier of the "east coordinate" variable
`elevator`	Identifier of the "elevator deflection" variable
`deg`	Degree
`g_factor`	Identifier of the "normal g-factor" variable
`height`	Identifier of the "flight height" variable
`km/h`	Kilometer per hour
`m`	Meter
`m/s`	Meter per second
`pitch`	Identifier of the "pitch angle" variable
`rudder`	Identifier of the "rudder deflection" variable
`s`	Second
`sideslip`	Identifier of the "sideslip angle" variable
`time`	Identifier of the "flight time" variable
`V_IAS`	Identifier of the "indicated airspeed" variable
`VR`	Aircraft rotation speed
`vert*`	Identifier of the "vertical velocity" variable
`Zadeh`	Identifier of the "L.Zadeh's membership function" variable
A	'Amber' safety color/zone
AI	Artificial Intelligence
B	'Black' safety color/zone
C.G.	Center of gravity
flaps	Flaps setting
FSI	Flight Safety Index
G	'Green' safety color/zone
L>>R	From left to right (crosswind direction)
L-system	A Lindenmayer system
max	Operation of selecting the 'hottest', at a given time instant, safety color
mass	Aircraft mass
PC	Personal computer
R	'Red' safety color/zone
T&E	Test and Evaluation
VATES	Virtual Autonomous Test and Evaluation Simulator (a proprietary software tool [4])
VFT&E	Virtual Flight Test and Evaluation
W	'White' or 'gray' safety color/zone
xx	Unspecified numeric value
АП	Авиационные Правила (Russian Airworthiness Regulations)